A protease-mediated mechanism regulates the cytochrome c_6/ plastocyanin switch in *Synechocystis* sp. PCC 6803

Raquel García-Cañas[1,2], Joaquín Giner-Lamia[1,3], Francisco J. Florencio[1,2] and Luis López-Maury*[1,2].

1. Instituto de Bioquímica Vegetal y Fotosíntesis, Universidad de Sevilla- CSIC, c/Américo Vespucio 49, 41092 Sevilla, Spain.

2. Departamento de Bioquímica Vegetal y Biología Molecular, Facultad de Biología, Universidad de Sevilla, Avenida Reina Mercedes s/n, 41012 Sevilla, Spain

3. Present address: Centro de Biotecnología y Genómica de Plantas UPM – INIA Parque Científico y Tecnológico de la U.P.M. Campus de Montegancedo, Autopista M-40, Km 38, Pozuelo de Alarcón, Madrid 28223, Spain

* Luis López-Maury

Email: llopez1@us.es

Tel: +34 954489501 ext. 909103

Raquel García-Cañas, ORCID 0000-0003-0062-6620; Joaquín Giner-Lamia, ORCID 0000-0003-1553-8295; Francisco J. Florencio, ORCID 0000-0002-2068-7861; Luis López-Maury, ORCID 0000-0002-3510-0621

Classification

Biological Sciences/Plant Biology

Keywords

Cyanobacteria, plastocyanin, cytochrome c_6

Author Contributions

Author contributions: R.M.G.C., J.G.L., F.J.F. and L.L.M. designed the research; R.M.G.C., J.G.L. and L.L.M. performed the research; R.M.G.C., J.G.L., F.J.F. and L.L.M. analyzed the data; L.L.M. wrote the manuscript with contributions from all authors.

Abstract

After the Great Oxidation Event (GOE), iron availability was greatly decreased and photosynthetic organisms evolved several alternative proteins and mechanisms. One of these proteins, plastocyanin, is a type I blue-copper protein that can replace cytochrome c_6 as a soluble electron carrier between cytochrome b_6f and photosystem I. In most cyanobacteria, expression of these two alternative proteins is regulated by copper availability, but the regulatory system remains unknown. Herein, we provide evidence that the regulatory system is composed of a BlaI/CopY family transcription factor (PetR) and a BlaR membrane protease (PetP). PetR represses *petE* (plastocyanin) expression and activates *petJ* (cytochrome c_6), while PetP controls PetR levels *in vivo*. Using whole-cell extracts, we demonstrated that PetR degradation requires both PetP and copper. Transcriptomic analysis revealed that the PetRP system regulates only four genes (*petE*, *petJ*, *slr0601*, and *slr0602*), highlighting its specificity. Furthermore, the presence of *petE* and *petRP* in early branching cyanobacteria indicates that acquisition of these genes could represent an early adaptation to decreased iron bioavailability following the GOE.

Significance Statement

After the appearance of oxygenic photosynthesis, Fe became oxidized and its solubility and availability were greatly decreased. This generated a problem for

most organisms since they are strongly dependent on Fe, especially photosynthetic organisms. In response, organisms evolved alternatives to Fe-containing proteins such as plastocyanin, a copper protein that substitutes for cytochrome c_6 in photosynthesis. Expression of these two proteins in cyanobacteria is regulated by Cu availability, but the regulatory system remains unknown. Herein, we describe the regulatory system for these alternative proteins in photosynthesis in cyanobacteria. The mechanism involves a transcription factor (PetR) and a membrane protease (PetP) that degrades PetR in the presence of Cu.

Main Text

Introduction

Cyanobacteria are prokaryotes that perform oxygenic photosynthesis, and their appearance on earth led to a dramatic increase in oxygen in the atmosphere. Although the timing of the Great Oxygenation Event (GOE) is well established, its extent is still a matter of dispute (1–4). The GOE caused a massive extinction because oxygen was toxic to most life forms (5, 6) and provoked Fe oxidation (Fe^{2+} to Fe^{3+}), which made Fe much less available since Fe^{3+} precipitates. This created an additional problem for all forms of life because Fe was already established as a major cofactor in biochemical reactions (7, 8). In fact, photosynthesis has high Fe requirements and photosynthetic organisms usually have a higher Fe quota than non-photosynthetic organisms because Fe is contained in proteins of both photosystems, in the cytochrome b_6f complex, in the soluble thylakoid lumen electron carrier cytochrome c_6 (Cytc_6), and in ferredoxin outside the thylakoids (9). Nowadays, Fe is a limiting nutrient in most ecosystems, especially in aquatic environments (10). Consequently, photosynthetic organisms evolved several alternatives to iron-containing proteins. In most cyanobacteria and some algae, Cytc_6 can be replaced by plastocyanin (PC), a type I blue-copper protein that acts as a thylakoid lumen soluble electron transporter. These two electron carriers are present in millimolar concentrations inside the thylakoid lumen (11), where Cytc_6 is replaced by PC, and this substantially reduces the requirement for Fe. In addition, PC uses Cu

87 which is much more soluble (and therefore available) than Fe in an oxidizing
88 atmosphere. Interestingly, plants have only retained PC for photosynthetic
89 electron transfer (12).

90 Expression of these two alternative electron carriers is regulated by
91 copper availability in both cyanobacteria and algae (13–15). The regulatory
92 system has been well characterized in the green alga *Chlamydomonas*
93 *reinhardtii*. CRR1, an SQUAMOSA promoter binding protein-like transcription
94 factor (SBP), activates *CYC6* (encoding Cytc_6) expression in response to copper
95 limitation (16). CRR1 is able to bind both Cu^{+} and Cu^{2+}, with the latter inhibiting
96 the DNA-binding ability of the SBP domain (16). However, the regulatory system
97 has not been identified in cyanobacteria, even though the Cytc_6/PC switch was
98 discovered more than 40 years ago (13, 14, 18–21), and it is frequently used to
99 control the expression of genes in several model systems (22–24). The switch
100 responds to the presence of copper at the transcriptional level; *petJ* (encoding
101 Cytc_6) is repressed while *petE* (encoding PC) is induced (18, 21, 25–27). Several
102 regulatory systems that respond to copper have been described in cyanobacteria
103 including CopRS (25, 27), InrS (27, 28), and BmtR (29), but none are involved in
104 regulating these two genes.

105 Herein, we unveiled the regulatory mechanism for the Cytc_6/PC switch in
106 cyanobacteria. It involves two genes: one encoding a transcription factor of the
107 BlaI superfamily (PetR) that binds to both *petE* and *petJ* promoters, repressing
108 *petE* and activating *petJ* in the absence of copper. The second gene encodes a

protease (PetP) that degrades PetR in response to copper. PetR degradation is activated by copper and requires PetP and copper *in vivo* and in an *in vitro* assay system, suggesting that PetP is responsible for PetR degradation. The system is widespread in all cyanobacteria, including early-branching cyanobacteria such as *Gloeobacter* and *Pseudoanabaena*, with the exception of most strains of the *Synechococcus*/*Prochlorococcus* groups.

Results

A BlaI/CopY homolog regulates the *petJ*/*petE* switch in *Synechocystis*

Bioinformatics analysis of genes within the vicinity of *petE* and *petJ* in 169 cyanobacterial genomes revealed that a transcription factor of the BlaI/CopY family (renamed PetR) was associated with *petJ* and/or *petE* genes in 13 genomes (SI Appendix, Figure S1). Although the overall number of genomes with this gene association was low, co-occurrence of *petR* with both *petE* and *petJ* was higher. Specifically, 75% of genomes harboring *petE* and *petJ* also contained *petR* (and a linked gene encoding a BlaR homolog; see below; SI Appendix, Figure S1), and these two genes were only present in genomes containing *petE* and *petJ* (SI Appendix, Figure S1; Supplementary dataset S1) with a few exceptions. This raised the possibility that *petR* could be related to the *petE*/*petJ* switch. In order to test this hypothesis, a mutant in the *slr0240* gene encoding PetR in *Synechocystis* sp. PCC 6803 (*Synechocystis* hereafter) was generated (PETR strain). The mutant strain fully segregated (SI Appendix, Figure

S2) and the phenotype was indistinguishable from that of the wild-type (WT) strain on BG11C plates (the standard defined medium for cyanobacteria; see below). Expression of *petJ* and *petE* genes was analyzed by RNA blot in both WT and PETR strains after copper addition to cells grown in BG11C lacking Cu (BG11C-Cu). In WT cells, *petE* was induced in response to copper and *petJ* was repressed (Figure 1A), as previously described (18, 25–27). By contrast, in the PETR strain *petE* was expressed even in the absence of copper and *petJ* was not expressed under any conditions (Figure 1A). Conversely, *copM* expression, which is induced in response to copper (25, 30), was similar in both strains. At the protein level, PC was induced in WT cells upon copper addition, while Cytc_6 abundance decreased after 4 and 24 h. CopM levels increased after copper treatment, with the unprocessed form of the protein accumulating first, followed by the processed at later timepoints (Figure 1B). By contrast, Cytc_6 was not detected under any conditions in the PETR strain, and PC was detected even in BG11C-Cu medium (Figure 1B). An increase in PC levels was still evident in the PETR strain after copper addition (Figure 1B), probably due to an increase in copper-bound PC, which is more stable than apoPC (25), since mRNA levels did not change after copper addition (Figure 1A). No changes in the CopM induction pattern were observed (Figure 1B). When an additional copy of *petR* was introduced in the PETR strain, either under its own promoter (PETR2 strain) or under the strong *cpcB* promoter (PETR3 strain), a WT phenotype was restored (SI Appendix, Figure S3). This indicates that *petR* was the only gene responsible for regulating these two genes. Similar results were obtained when protein levels

were analyzed in steady-state cells of the WT strain grown in media with differences in copper availability. PC was high in copper-containing medium (BG11C 330 nM Cu), lower in BG11C-Cu (~30 nM Cu), and much lower in BG11C-Cu+ bathocuproinedisulfonic acid (BCSA), a copper-specific chelator (no copper; Figure 1C). The PETR strain expressed PC in all conditions, but accumulated higher levels in copper-containing media. Meanwhile, Cytc_6 was not detected in the PETR strain in any media, and WT cells displayed higher levels in BG11C-Cu+BCSA than in BG11-Cu (Cytc_6 was almost undetectable in copper-containing medium; Figure 1D).

Slr0241(PetP) is also involved in *petJ*/*petE* regulation

Downstream of *petR* there is another gene (*slr0241*, herein named *petP*) that encodes an M48/M56 superfamily of proteases (Pfam families PF01435 and PF05569). The *petP* start codon overlaps with the stop codon of *petR*, and both genes were expressed as a single transcriptional unit (SI Appendix, Figure S4). Analysis of the PetP sequence using TMHMM 2.0 software (31) predicted four transmembrane helices (residues 4–21, 28–50, 65–87, and 256–278), a 14 residue loop connecting TM2 and TM3, and a cytoplasmic domain (88-256) that contains the HEXXH conserved catalytic motif (SI Appendix, Figure S5). This domain organization is very similar to that of BlaR from *Staphylococcus aureus* (32), which is involved in regulating β-lactam resistance by degrading BlaI, although it lacks the C-terminal periplasmic domain that binds to β-lactams. Furthermore, the organization of *petRP* is conserved in all cyanobacterial

genomes (SI Appendix, Figure S1, and Supplementary dataset S1), suggesting that both genes might be functionally related. To test this hypothesis, we mutated the *petP* gene. The resulting mutant strain (PETP) was viable (SI Appendix, Figure S2) and exhibited a similar growth phenotype to the WT strain on BG11C plates (see below). When gene expression was tested in this mutant, *petE* was repressed both in the presence and absence of copper, while *petJ* was expressed constitutively (Figure 1A). The same results were observed at the protein level, with Cytc_6 detected both in the presence and absence of copper, while PC was undetectable under any conditions (Figure 1B). When steady-state proteins levels were analyzed in different copper-containing media, PC was not detected in the PETP strain in any media, while Cytc_6 was detected in all media. Despite this, Cytc_6 levels were lower in copper-containing medium than in media lacking copper (Figure 1D). These results indicate that *petP* is involved in the regulation of both genes, acting in an opposite way to *petR*. A double mutant lacking both *petR* and *petP* genes was also generated (PETRP; SI Appendix, Figure S2). The PETRP strain displayed the same phenotype as the PETR strain (SI Appendix, Figure S6), revealing that *petP* acts upstream of *petR*.

PetP regulates PetR levels in response to copper

Given that PetP belongs to the M48/M56 superfamily of proteases, this protein might regulate PetR through proteolysis. To investigate this hypothesis, we generated an antiserum against PetR that allowed us to monitor PetR protein

198 abundance in response to copper. In the WT strain, PetR was detected in cells
199 cultivated in BG11C-Cu, and it was rapidly degraded after copper addition, since
200 *petRP* mRNA levels did not change following copper addition (SI Appendix,
201 Figure S4). Two bands were detected (~15 kDa and ~12 kDa, Figure 2A),
202 suggesting an initial and specific cut, and subsequent degradation of the
203 fragments. Indeed, in order to consistently detect PetR, whole cells were loaded
204 onto gels (see Materials and Methods) because PetR was quickly degraded
205 during protein extract preparation. The best studied homologs of PetRP are
206 BlaIR proteins involved in antibiotic resistance from *S. aureus* (32). Processing
207 of these proteins was initially identified in BlaI, it takes places after Phe100 in the
208 amino acid sequence, and is completely conserved in all cyanobacterial PetR
209 proteins (SI Appendix, Figure S7). As expected, the theoretical molecular mass
210 of the fragment generated by this digestion was consistent with the expected size
211 detected by immunoblotting (Figure 2A and SI Appendix, Figure S7; expected
212 sizes of full-length and processed proteins are 15.80 and 12.38 kDa,
213 respectively). In contrast to the WT strain, PetR levels did not change in
214 response to copper in the PETP strain (Figure 2). Therefore, the initial cleavage
215 is probably mediated by PetP, and the fragments are probably further degraded
216 by other unspecific proteases. As expected, PetR was not detected in the PETR
217 strain (Figure 2 and SI Appendix, Figure S3E). When PetR protein abundance
218 was analyzed in steady-state cultures grown in different copper regimes, levels
219 were clearly regulated in the WT strain, since they were higher in the presence of
220 BCSA than in BG11-Cu, and not detected in copper-containing media (Figure 2B

and C). PetR levels were higher in the PETP strain than in the WT strain, even when WT cells were cultured in the presence of BCSA, although levels were decreased slightly at higher copper availability (Figure 2B and C). These results are consistent with the Cytc_6 and PC levels measured under the same conditions (Figure 1C and D), and demonstrate that PetR protein abundance is regulated by PetP *in vivo* according to Cu availability.

PetP degrades PetR directly in a copper-dependent manner

To further characterize this regulation, we performed an *in vitro* degradation assay in which recombinant GST-PetR was incubated with total cell extracts from WT, PETR, and PETP strains, and GST-PetR processing was followed by immunoblotting. GST-PetR was not degraded by whole-cells extracts prepared from WT, PETP, or PETR strains when copper was not added to the extracts (Figure 2D). In contrast, when copper was added to extracts, GST-PetR was degraded by WT and PETR extracts, but not by PETP extracts, indicating that a PetP-mediated PetR degradation was activated by copper (Figure 2D).

To confirm that PetP was directly involved in PetR degradation, and that this degradation was not mediated by an additional protein from *Synechocystis*, *petRP* genes under their own promoter were cloned in a plasmid and transformed into *E. coli*. Total extracts were prepared from cells carrying a plasmid containing *petRP* or an empty plasmid, and degradation of GST-PetR was monitored. The results were similar to those obtained using total extracts from *Synechocystis*: GST-PetR was degraded in total extracts prepared from

244 cells containing a plasmid that includes *petRP*, but not in extracts prepared from
245 the strain carrying an empty plasmid (Figure 2E). PetR degradation also required
246 copper supplementation of extracts, demonstrating that PetR degradation
247 depends on this metal (Figure 2E). These results also showed that PetP can
248 degrade PetR directly without the participation of any other protein from
249 *Synechocystis*. Thus, PetP controls PetR levels directly via a copper-dependent
250 mechanism.
251
252 **PetR binds to both *petE* and *petJ* promoters**
253 In order to establish whether PetR regulates *petJ* and *petE* directly, we
254 performed Electrophoretic Mobility-Shift assays to analyze PetR binding to both
255 promoter regions. As a first approach, we carried out band shift assays using a
256 recombinant version of PetR (see Materials and Methods for details) and two
257 probes corresponding to the *petJ* and *petE* promoters. PetR was able to bind to
258 both promoters (Figure 3A and B), and the binding was not affected by Cu (Cu^{+}
259 or Cu^{2+}; SI Appendix, Figure S8). PetR exhibited a higher affinity toward *petE*
260 than the *petJ* promoter, and was able to completely titrate the probe at lower
261 concentrations (Figure 3A and B). These results indicate a dual role for PetR
262 activating *petJ* expression and repressing *petE*.
263 In order to identify the PetR binding site, we carried out a bioinformatic
264 analysis of the *petE* and *petJ* promoters in cyanobacterial genomes. A 300-bp
265 fragment surrounding *petE* and *petJ* promoters was retrieved from genomes that
266 contained *petE*, *petJ,* and *petRP* using MGcV database (http://mgcv.cmbi.ru.nl/;

SI Appendix, Supplementary dataset S2). Analysis of the sequences of *petE* and *petJ* promoters using MEME suite revealed that the motif shown in Figure 3C was significantly enriched in both. This motif contains the $GACN_5GTC$ sequence, which was completely conserved, positioned 75 bp upstream from the starting ATG codon (and 37 bp from the tsp) in the *petJ* promoter, and at 118 bp from the ATG codon (and 23 bp from the tsp) in the *petE* promoter. In the *petJ* promoter, the putative binding site is centered around the -35 box in the promoter, in a location suitable as an activator site. In contrast, this sequence is located between the -10 and -35 boxes in the *petE* promoter, compatible with a repressor role of PetR. These locations are consistent with gene expression data obtained by RNA blotting (Figure 1) and transcriptomics analysis (see below) of PETR and PETP mutant strains, which suggests that PetR activates *petJ* and represses *petE* expression. Notably, when MEME analysis was repeated using only *petJ* promoters, an extended motif was identified (Figure 3D). This motif includes the core of the motif shown in Figure 3C, but also two direct repeats of the sequence TTTGAC-N_9-TTTGAC (Figure 3D). A different motif was also identified when the same analysis was performed using only *petE* promoter sequences (Figure 3E). This motif includes the core motif shown in Figure 3C, but in an extended form of the inverted repeat GACA-N_3-TGTC. However, the *Synechocystis* sequence in the *petE* promoter is GACG-N_3-TGTC (Figure 3F).

RNA-seq analysis of the PetR regulon

To fully characterize the PetR regulon, RNA-seq was carried out using RNA extracted from WT, PETR, and PETP strains grown in BG11C-Cu, and 2 h after addition of 0.5 μM Cu addition (SI Appendix Supplementary dataset S3). Using a threshold of at least a 2-fold change and P_{adj} < 0.01, 14 genes were induced (*petE,* both plasmid and chromosomal copies of *copMRS, copBAC*, *and nrsBAC*) and three were repressed (*petJ, slr0601, and slr0602*) in the WT strain after copper addition (SI Appendix, Table S1; Supplementary dataset S4), in agreement with previous microarray analysis (27). A similar response was observed in the PETR strain with *copMRS* (both copies)*, copBAC*, and *nrsBAC* operons, and three additional genes of unknown function were also differentially regulated (SI Appendix, Table S1). In the PETP strain, 16 genes were induced after copper treatment, including *copMRS* (both copies)*, copBAC*, and *nrsBAC* operons (SI Appendix, Table S1). As expected from the results shown in Figure 1, neither *petE* nor *petJ* were differentially expressed in PETR or PETP strains (SI Appendix, Figure S9). Furthermore, *slr0601* and *slr0602* were not differentially regulated in PETR or PETP (SI Appendix, Table S1). When gene expression was directly compared between WT and PETR strains, eight genes were differentially regulated in BG11C-Cu (seven expressed at higher levels in WT, and one downregulated), and six were differentially regulated after copper addition (SI Appendix, Supplementary dataset S4). As expected, this group of genes included *petRP* (*petR* was induced 5.93 and 4.73-fold, and *petP* was induced 37 and 38-fold for in BG11C-Cu and +Cu, respectively), *petE* (repressed 41-fold in -Cu and 2-fold in +Cu), and *petJ* (induced 168-fold in -Cu and 8.7-fold

312 in +Cu), as well as *slr0601*, *slr0602*, *slr0242*, *sll1796*, *sll0494*, and *slr1896* (SI
313 Appendix, Supplementary dataset S4). Similarly, when WT and PETP strains
314 were compared, only three genes were differentially regulated in BG11C-Cu (all
315 upregulated), and eight genes were differentially regulated in BG11C+Cu (also
316 upregulated). These genes included *petP* (upregulated 5-fold in both conditions
317 in WT), *petE* (also upregulated in WT, by 5.3-fold in -Cu and 116-fold in +Cu),
318 *petJ* (repressed 25-fold in +Cu), and *slr0242*, *slr0601*, *slr0602*, *slr1896*, and
319 *sll1926* (SI Appendix, Supplementary dataset S4). These results suggest that the
320 PetRP regulon comprises *petJ*, *petE*, *slr0601*, and *slr0602*, as these genes were
321 regulated by copper in WT cells, and affected in both PETR and PETP strains,
322 although with opposite patterns in the two mutant strains.

323 The *slr0601* and *slr0602* genes are linked in the genome and probably
324 form an operon (SI Appendix, Figure S10A). Expression of *slr0601* was analyzed
325 by RNA blotting, and the pattern was similar to that of *petJ*: repressed after
326 copper addition in WT, not expressed in PETR, and constitutively expressed in
327 PETP strains (SI Appendix, Figure S10B). Furthermore, PetR could bind to the
328 promoter sequence of *slr0601* (SI Appendix, Figure S10C), which contains a
329 sequence matching the one identified in Figure 3 (SI Appendix, Figure S10D).
330 Together, these results indicate that the *petRP* regulon is only composed of *petJ*,
331 *petE*, and *slr0601-slr0602* in *Synechocystis*.

332

333 **Physiological characterization of PETR and PETP mutant strains**

All mutants generated in this study were fully segregated in BG11C, and were able to grow in BG11C-Cu, but given their gene expression programs (Figures 1 and 2; SI Appendix, Figure S9; Table S1, supplementary dataset S4), growth defects were expected in different copper regimes. We analyzed the growth of the PETR and PETP strains on plates differing in copper availability: BG11C-Cu+BCSA (no copper), BG11C-Cu (~30 nM Cu), and BG11C (330 nM Cu). PETR was only affected in BG11C-Cu containing BCSA, similar to the PETJ strain, which has an interrupted *petJ* gene (Figure 4A). By contrast, the PETP strain was not affected under any conditions (Figure 4), because it expressed *petJ* in all tested conditions (Figure 1). Finally, the PETE strain showed a decreased growth rate (but survived) in BG11C, as previously reported (25, 26, 33) (Figure 4A and SI Appendix, Figure S11). A double mutant lacking both genes (PETRP strain) was indistinguishable from the single mutant PETR (Figure 4A and SI Appendix, Figure S6). Analysis of photosynthetic activity revealed that PETJ and PETR strains reached lower oxygen evolution rates (16.8 ± 0.3 μmol min^{-1}/OD_{750nm} and 18.9 ± 0.75 μmol min^{-1}/OD_{750nm}, respectively) than WT (23 ± 3.82 μmol min^{-1}/OD_{750nm}), PETE (24.5 ± 2.46 μmol min^{-1}/OD_{750nm}), and PETP (23.2 ± 5 μmol min^{-1}/OD_{750nm}) strains when cultured in BG11c-Cu+BCSA, although they saturated at the same light intensity (Figure 4B). When cultured in BG11C, the PETE strain exhibited a severe defect in oxygen evolution (reaching only 5.3 ± 2.7 μmol min^{-1}/OD_{750nm} and saturating at a light intensity of 180 μmol $m^{-2}s^{-1}$(Figure 4C). Surprisingly, the PETP strain exhibited a lower maximum capacity, reaching only 13.24 ± 2.63 μmol min^{-1}/OD_{750nm}, while WT

(24.11 ± 3.66 μmol min^{-1}/OD_{750nm}), PETJ (22.25±4.34 μmol min^{-1}/OD_{750nm}), and PETR (21.87 ± 4.36 μmol min^{-1}/OD_{750nm}) strains all reached similar levels, equivalent to those observed in BG11C-Cu (Figure 4C). Despite this, all strains saturated at the same light intensity (500 μmol $m^{-2}s^{-1}$). The PETP strain expressed *petJ* constitutively (Figures 1 and 2), and was therefore not expected to show any photosynthetic defect.

Genetic interactions between *petRP*, *petJ*, and *petE*

Our results show that *petRP* is the main system responsible for the *petJ*/*petE* switch following copper addition. Either *petJ* or *petE* are required for photosystem I (PSI) reduction, and therefore for the growth of cyanobacteria (33), despite early studies showing growth of *Synechocystis* in the absence of both proteins (34). The results presented in Figures 1 and 4 suggest that the low levels of PC present in BG11C-Cu (even in the presence of BCSA) were enough to sustain growth of PETR and PETJ mutant strains, albeit at decreased rates (Figure 4A). Furthermore, although the PETE strain showed impaired growth in the presence of copper (Figure 4A), it was able to grow at decreased rates because all cells grew after prolonged incubation (SI Appendix, Figure S11), probably due to low levels of Cytc_6. Moreover, a double mutant lacking functional *petE* and *petR* genes (or both *petR* and *petP*, strain PETERP) could not be completely segregated (SI Appendix, Figure S12), probably due to low expression levels of *petJ* in the absence of PetR (Figures 1A and SI Appendix, Figure S9), reinforcing

379 the idea that at least one of the soluble transporters (even at low levels) is
380 needed in *Synechocystis*. By contrast, a double mutant lacking *petE* and *petP*
381 (PETEP) was able to grow at WT rates in the presence of copper (SI Appendix,
382 Figure S11 and S12). Consistently, the double mutant PETJP did not segregate,
383 while PETJR and PETJRP mutants fully segregated (SI Appendix, Figure S12).
384 Together, these results suggest that a double mutant lacking both *petJ* and *petE*
385 should not be viable. To test this hypothesis, a double mutant was generated by
386 transforming the PETE mutant with pPETJCm. Merodiploid colonies were
387 obtained, but they never segregated completely (SI Appendix, Figure S13),
388 despite subculturing under several light regimes for more than 2 years. To
389 confirm that PC and Cytc_6 were expressed in slow-growing mutants, we used
390 concentrated extracts and loaded 150 µg of total protein per lane. Cytc_6 was
391 detected at low levels in WT and PETE strains, but not in the PETR strain, in the
392 presence of copper (SI Appendix, Figure S12). In WT, PETR, and PETJ strains,
393 PC was detected (although at low levels; Figures 1, 2, and SI Appendix, Figure
394 S12) in the absence of Cu, therefore allowing growth of these strains at
395 decreased rates (Figure 4).

396

397 **Discussion**

398 Acquisition of PC as an alternative electron carrier was probably an early
399 adaptation after oxygenic photosynthesis appeared, since local oxygenation
400 (even before the GOE) presumably decreased Fe availability. This is reinforced

401 by the presence of both electron carriers in early-branching cyanobacteria such
402 as *Gloeobacter* and *Pseudoanabaena* (SI Appendix, Figure S1, Supplementary
403 dataset 1). Although known about for more than 40 years (13, 14), the regulatory
404 system responsible for the *petJ*/*petE* switch in cyanobacteria remained
405 undiscovered. Herein, we show that the *petRP* genes are responsible for this
406 regulation (Figures 1 and 5). The system seems to have been acquired early
407 during evolution, because like *petE*, it is present in early branching
408 cyanobacteria, and it is widespread in most cyanobacterial clades (SI Appendix,
409 Figure S1). The only exception is the *Synechococcus*/*Prochlorococcus* clade, in
410 which most strains lack *petRP* genes, similar to previous observations on other
411 regulatory systems (35). We showed that *petRP* act in a single pathway in which
412 PetR positively regulates *petJ* and negatively regulates *petE*, while PetP
413 regulates PetR protein levels in response to copper (Figure 5). PetR directly
414 regulates *petE* and *petJ* gene expression by binding to the promoter regions of
415 these two genes (Figure 3). However, the affinity for both promoters is differs
416 markedly, with the *petJ* promoter requiring much higher PetR concentrations for
417 binding than the *petE* promoter *in vitro*. In addition, binding sites are in different
418 locations in the two promoters, replacing the -35 box in *petJ* and between -10
419 and 35 in *petE*, consistent with an activating role in *petJ* and a repressing role in
420 *petE*, as confirmed by gene expression analysis (Figures 1, 2 and 5; SI
421 Appendix, Figure S9, Table S1, supplementary dataset S4).

Furthermore, our bioinformatics analysis identified an inverted repeat as the core binding site for both promoters in cyanobacteria (Figure 3C), but when *petJ* and *petE* promoters were used, variations of the motif were identified (Figure 3D and E). Given that the protein abundance of PetR *in vivo* depends on copper concentration (Figure 2), and binding to the *petJ* (and *slr0601*) promoter requires higher PetR concentrations (Figure 3 and SI Appendix, Figure S10), *petJ* will only be fully activated when all copper is exhausted (and PetR accumulates at high levels), preventing induction of *petJ* if some copper remains available for PC synthesis. Although BlaI/CopY homologs have been reported to act only as repressors, our results strongly suggest that PetR acts as an activator for *petJ* expression (Figures 1, 3, and SI Appendix, Figure S9B; Table S1). This indicates that BlaI/CopY homologs may also act as activators, as suggested previously (36). Since the binding sites for PetR activation are different to the repressor sites (Figure 3), it is possible that they have remained elusive when studying PetR homologs (37). This dual role for DNA binding proteins that were initially considered to be repressors has been uncovered recently in proteins such as Fur, which was believed to be an activator in both its apo and holo forms (38–40).

Our RNA-seq analysis revealed that only four genes are under the control of the *petRP* system in *Synechocystis*: *petE*, *petJ*, *slr0601*, and *slr0602* (SI Appendix, Figures S9 and S10; Table S1). Inspection of the promoter sequences of these four genes reveals conservation of the core sequence, identified using

444 GACN$_5$GTC in the *petJ* and *petE* promoters, but also using only *petJ* promoter
445 sequences (Figure 3 and SI Appendix, Figure S10). The *slr0601* and *slr0602*
446 genes encode two small proteins restricted to cyanobacteria that share low
447 sequence conservation. Slr0601 contains two transmembrane domains with both
448 C-terminal and N-terminal regions predicted to be cytoplasmic, while Slr0602
449 contains a coiled-coil region but no other recognizable domains. The low levels of
450 sequence conservation and the lack of known domains make it difficult to assign
451 putative functions for these two proteins.

452 PetP belongs to the M48/M56 family of proteases, and we showed that
453 this protein regulates PetR by controlling its protein abundance in response to
454 copper *in vivo*. This regulation is probably direct as we showed that recombinant
455 PetR is degraded *in vitro* by both *Synechocystis* and *E. coli* extracts, and that this
456 degradation depends on the presence of PetP and copper (Figure 2). This
457 regulatory system is homologous to the BlaI/BlaR regulatory system that
458 regulates β-lactamase expression in *S. aureus*. We explored the mechanism by
459 which copper is sensed by PetRP. PetR belongs to the BlaI/CopY family of
460 transcription factors, and CopY proteins have been demonstrated to bind copper
461 directly (41). Therefore, it is possible that PetR may bind copper, and although
462 this binding may not affect its DNA binding activity (SI Appendix, Figure S8), it
463 may alter its conformation, making it more susceptible to degradation by PetP.
464 Nevertheless, CopY copper binding sites are not conserved in PetR (28), making
465 this hypothesis unlikely.

BlaR/MecR contains a C-terminal extra-cytoplasmic domain that is acylated by β-lactam antibiotics, and this modification activates BlaR, which subsequently degrades BlaI. This domain is absent in PetP, and therefore copper sensing must be mediated by a different domain. The loop between the second and third transmembrane domains of PetP includes two methionine residues (M53 and M58 in *Synechocystis*) that are conserved in all PetP sequences (SI Appendix, Figure S5), which could be putative copper ligands. Interestingly, this domain in BlaR/MecR interacts with the periplasmic C-terminal domain after it binds to β-lactams (42–44). This interaction has been proposed to transduce the signal and activate the protease domain in BlaR. Therefore, these two methionine residues in PetP may bind copper and transduce the signal in a similar way.

Moreover, as PetP is an integral membrane protein, it would be interesting to identify which cyanobacterial membrane system this protein targets. Most copper in *Synechocystis* is presumably sequestered in the thylakoids, where it is bound to PC (45, 46), and CopS, the sensor protein in the copper resistance system, is located to both plasma and thylakoid membranes (25). If PetP is also targeted to both membrane systems, this could allow PetP to respond not only to an external surplus of copper, but also when the metal is released from internal PC. PetP localization to the thylakoids is reinforced by the fact that mutants lacking the P_1-type-Cu-ATPases CtaA, PacS, or both (which are involved in Cu acquisition by PC) displayed decreased levels of *petE* mRNA after copper

addition (25, 47). This suggests that Cu needs to be transported to the thylakoid in order to be detected by the PetRP system.

Furthermore, our results showed that *Synechocystis* can synthesize PC even when copper levels are very low due to the presence of BCSA in BG11C-Cu. This indicates that some copper can be transported even in the presence of BCSA, suggesting that the copper import system (which remains unidentified) has a higher affinity for copper than the chelating agent. Accumulation of PC in the presence of BCSA was only observed in the PETR strain in which *petE* expression was constitutive (Figures 1, 5, and SI Appendix, Figure S9), because in the WT strain *petE* is repressed and PC cannot be synthesized, even if copper is available.

Finally, our results also suggest that there are other layers of regulation at the posttranscriptional level because Cytc_6 and PC protein abundance does not always correlate with mRNA levels. PC was more abundant in Cu-containing media in the PETR strain in which *petE* mRNA levels did not change in response to copper (Figure 1). Similarly, Cytc_6 levels were decreased in the PETP strain after copper addition, even when mRNA levels were not decreased. PC protein abundance may be related to the protein not being correctly translated and/or folded in the absence of available copper, or due to degradation of the apoprotein, but synthesis of Cytc_6 should not be altered by copper. It has been proposed that IsaR sRNA regulates *petJ* translation in response to Fe deprivation (24). We did not find *isaR* to be differentially regulated in our RNA-seq

experiment (SI Appendix, Figure S14), hence it is unlikely that this regulation is mediated by *petRP*. Furthermore, oxygen evolution was affected in the PETP strain (which expresses Cytc_6; Figure 4C) in the presence of copper, suggesting that additional changes in the photosynthetic transport chain might be present, as reported for *Chlamydomonas* (48). Finally, although single mutants of either *petJ* or *petE* were able to grow, even in a copper regime in which expression of the other gene was repressed, these strains exhibited growth and photosynthesis defects (Figure 4), in agreement with previous studies (33, 49–51). Double mutants of both *petJ* and *petE* were not viable (SI Appendix, Figure S13), and double mutants lacking one of the genes encoding the electron transport proteins and with decreased expression of the other due to the lack of *petP* (constitutive repression of *petE;* strain PETJP) or *petR* (unable to induce *petJ*; strain PETER) were not viable either (SI Appendix, Figure S12). Together, these results demonstrate that *petRP* are essential for expression of these genes, and that levels of PC or Cytc_6 proteins must be above a critical threshold for survival of the strains. These results also rule out the existence of another electron transfer mechanism between cytochrome b_6f and PSI.

Materials and Methods

Strains and culture conditions

All *Synechocystis* strains used in this work were grown photoautotrophically on BG11C (52) or BG11C-Cu (lacking $CuSO_4$) medium at 30ºC under continuous

532 illumination using 4000–4500 K white-LED light (50 µmol photon m^{-2} s^{-1},
533 measured at the flask surface) and bubbled with a stream of 1% (v/v) CO_2 in air.
534 BG11C-Cu was supplemented with 300 µM BCSA as a chelating agent to trap
535 any trace of copper, when required. For plate cultures, media were
536 supplemented with 1% (w/v) agar. Kanamycin, nourseothricin, chloramphenicol,
537 spectinomycin, and erythromycin were added to a final concentration of 50 µg
538 mL^{-1}, 50 µg mL^{-1}, 20 µg mL^{-1}, 5 µg mL^{-1}, and 5 µg mL^{-1}, respectively.
539 Experiments were performed using cultures from the logarithmic phase (3–4 µg
540 chlorophyll mL^{-1}). *Synechocystis* strains are described in SI Appendix, Table S2.

541 *E. coli* DH5α cells were grown in Luria Broth or M9 (supplemented with 1
542 mL LB per L of M9) media and supplemented with 100 µg mL^{-1} ampicillin, 50 µg
543 mL^{-1} kanamycin, 50 µg mL^{-1} nourseothricin, 20 µg mL^{-1} chloramphenicol, and
544 100 µg mL^{-1} spectinomycin when required.

545 *Insertional mutagenesis of Synechocystis genes*

546 For *slr0240* (*petR*) mutant construction, a 1524-bp fragment was amplified using
547 oligonucleotides 223 and 224, cloned into pSPARKII (generating pPETR), and a
548 Sp^R cassette was inserted in the *Eco*RV site at codon 31 in the *slr0240* open
549 reading frame (ORF), generating plasmid pPETR_Sp. For the *slr0241* (*petP*)
550 mutant, a 970-bp fragment was amplified using oligonucleotides 248 and 249
551 and cloned into pSPARKII, generating pPETP. A 582-bp *Nhe*I fragment was
552 substituted by an *Xba*I erythromycin cassette, generating pPETP_Ery. For the
553 *petRP* double mutant, a 1492-bp fragment was amplified by PCR using

554 oligonucleotides 256 and 257, and cloned into the pSPARKII vector, generating
555 the pPETRP plasmid. A 650-bp *Bst*EII fragment from plasmid pPETRP was
556 substituted by an *Hin*cII-digested SpR cassette from pRLSpec, generating
557 pPETRP_Sp. To generate the *petJ* mutant, a 1023-bp fragment was amplified
558 using oligos 235 and 236, and cloned into pSPARKII, generating pPETJ, and a
559 *Xba*I CC1 Cm resistance cassette was inserted in the *Nhe*I site present in the
560 *petJ* ORF, generating pPETJ_Cm. For PETR complementation, a 639-bp
561 fragment (185 bp upstream of the *petR* STOP codon) was amplified using
562 oligonucleotides 256 and 234, and cloned into pGLNN digested with *EcoR*I and
563 *Not*I, generating pPETR_comp. For the PETR3 strain, a 463-bp fragment was
564 amplified using oligonucleotides 258 and 234 (adding *Sal*I and the pET28
565 ribosome binding site upstream of *petR* ATG), digested with *Sal*I-*Not*I, and
566 cloned into pGLN-PcpcB digested in the same way, generating pPETR_OE.
567 These plasmids were used to transform WT *Synechocystis*, PETR, PETE, or
568 PETJ strains, generating PETR, PETR2, PETR3, PETP, PETRP, PETER,
569 PETEP, PETERP, PETJR, PETJP, PETJRP, and PETEJ strains. Segregation of
570 the strains was verified by PCR with the appropriate primer pairs, as depicted in
571 SI Appendix, Figures S2, S3, S11, and S13. All plasmids were sequenced to
572 verify that no unwanted mutations were introduced. Sequences for all
573 oligonucleotides are listed in SI Appendix, Table S3.

574 *RNA isolation and RNA blot analysis*

575 Total RNA was isolated from 30 mL samples of *Synechocystis* cultures in the
576 mid-exponential growth phase (3 to 4 µg chlorophyll mL^{-1}). Extractions were
577 performed by vortexing cells in the presence of phenol-chloroform and acid-
578 washed baked glass beads (0.25–0.3 mm diameter) as previously described
579 (53). A 5 µg sample of total RNA was loaded onto each lane of a 1.2%
580 denaturing agarose formaldehyde gel (54), electrophoresed, and transferred to a
581 nylon membrane (Hybond N-Plus; GE Biosciences). Prehybridization,
582 hybridization, and washes were performed in accordance with the manufacturer's
583 instructions. Probes for RNA blot hybridization were synthesized by PCR using
584 oligonucleotide pairs 172-173, 174-175, 389-390, 275-276, 274-275, and 178-
585 179 (SI Appendix, Table S3) for *petE*, *petJ*, *copM*, *slr0601*, and *rnpB*,
586 respectively. DNA probes were ^{32}P-labeled with a random primer kit (Rediprime II
587 catalog #RPN1633; GE Biosciences) using [α-32P] dCTP (3,000 Ci/mmol).
588 Hybridization signals were quantified with a Cyclone Phosphor System
589 (Packard). Each experiment included at least three biological replicates.

590 *Immunoblotting*

591 For analysis, proteins were fractionated by SDS-PAGE and immunoblotted with
592 antibodies against plastocyanin (1:3000), cytochrome c_6 (1:3000), CopM
593 (1:7000), PetR (1:6000), or *Synechococcus* sp. PCC 6301 glutamine synthetase
594 I (1:100,000). ECL Prime (catalog # RPN2232, GE Biosciences) was used to
595 detect the different antigens with anti-rabbit secondary antibodies conjugated to
596 horseradish peroxidase (1:25,000; catalog # A0545, Sigma). Either photographic

597 film or a ChemiDoc Imaging System (Bio-Rad) were used for signal detection
598 and quantification.

599 Samples were prepared from whole cells or soluble extracts. For whole
600 cells, cells were harvested from cultures with an optical density at 750 nm
601 (OD_{750nm}) of 1, the supernatant was carefully removed, cells were resuspended in
602 100 µL of 1× Laemmli loading buffer, and boiled for 10 min. For soluble extracts,
603 Cells equivalent to 20 OD_{750nm} were collected, resuspended in 300 µL of buffer A
604 (50 mM TRIS HCl pH 8, 50 mM NaCl, 1 mM phenylmethylsulfonyl fluoride) and
605 broken using glass beads via two cycles, separated by 5 min on ice, of 1 min in a
606 minibead beater. Cell extracts were recovered from the beads and samples were
607 clarified by two sequential centrifugations: 5 min at 5000 *g* to eliminate cell
608 debris, and 15 min at 15,000 *g* to remove membranes. Protein concentrations in
609 cell-free extracts and purified protein preparations were quantified using Bradford
610 reagent (catalog # 5000006, Bio-Rad), with ovalbumin as a standard, and
611 specified amounts of protein were separated by SDS-PAGE.

612 *PetR protein purification*

613 The complete *petR* ORF was cloned from *Synechocystis* DNA after PCR
614 amplification with oligonucleotides 233 and 234, and cloned into the *Bam*HI-*Not*I
615 sites of pGEX6P, generating pGEX_PETR. The GST-PetR fusion protein was
616 expressed in *E. coli* DH5α cells. A 1 L culture was grown in Luria broth medium
617 to an OD_{600nm} of 0.6, cooled to 4ºC, 0.1 mM isopropyl-b-D-thiogalactopyranoside
618 (IPTG) was added, and culturing was continued at 25ºC overnight. Cells were

harvested by centrifugation, resuspended in 5 mL of PBS buffer (150 mM NaCl, 16 mM Na_2HPO_4, 4 mM NaH_2PO_4, 4 mM phenylmethylsulfonyl fluoride, 7 mM β-mercaptoethanol) supplemented with 0.1% Triton X-100, broken by sonication on ice, and insoluble debris was pelleted by centrifugation for 45 min at 25,000 *g*. Soluble extracts were mixed with 1 mL of glutathione agarose beads (catalogue number # 17075601, GE Healthcare) and incubated for 2 h at 4ºC with gentle agitation. Beads were transferred to a column and washed extensively with PBS buffer (20–30 column volumes) until no more protein was eluted from the column. The column was equilibrated with 10 volumes of 50 mM TRIS HCl pH 7.5, 150 mM NaCl, 1 mM EDTA, and 1 mM dithiothreitol, and beads were resuspended in two volumes of the same buffer. A 20 µL sample of Precission protease (2 U/µL; catalogue # 27084301, GE Healthcare) was added and beads were incubated overnight at 4ºC. Beads were poured into an empty column and the flow through fraction was collected. This fraction was diluted three times in 50 mM TRS HCl pH 8, and applied to a HiTrap Heparin column (catalogue # 17040601, GE Healthcare) connected to an Amersham FPLC system. The column was washed with 10 volumes of 50 mM TRIS HCl, 100 mM NaCl, and a 20 mL gradient from 0.1–1 M NaCl was applied. Fractions containing PetR were pooled and concentrated. GST-PetR fusion protein was eluted from glutathione agarose beads with 3 mL of 50 mM TRIS HCl pH 8 containing 10 mM reduced glutathione after washing the column with PBS. A gel of the purified fractions is shown in SI Appendix, Figure S15.

641 *Protease assays*

642 Cells equivalent to 20 OD_{750nm} of *Synechocystis* strains were harvested from mid-
643 exponential growth phase cultures, resuspended in 300 µL of buffer containing
644 50 mM TRIS-HCl pH 8, 50 mM NaCl, 10% glycerol, and 1 mM $ZnSO_4$, and
645 broken with 2 volumes of glass beads using a minibead beater. Total cell extracts
646 were collected by piercing the bottom of the tube with a needle. Extracts were
647 centrifuged for 5 min at 5000 *g* to remove the remaining glass beads and
648 unbroken cells, and the supernatant constituted the total extract. A 2-µg sample
649 of GST-PetR was added to 150 µL of total extracts (containing 150 µg of total
650 protein) and incubated at 30ºC. At the indicated times, 20 µL samples were
651 removed, mixed with 7 µL of 4× Laemmli buffer and boiled for 10 min. A 5 µL
652 sample was used for immunoblotting using α-PetR antibodies.

653 For *E. coli* assays, DH5α cells transformed with pN_petRP_Nat or pN_Nat
654 were grown to late exponential phase (OD_{595nm} 1–2), and cells at an OD_{595nm}
655 value of 20 were collected and processed as described above for *Synechocystis*.
656 The pN_petRP_Nat plasmid was constructed by excising a 1478-bp fragment
657 from pPETRP using *Eco*RI and *Xho*I, containing petRP and the 185-bp region
658 upstream from *petR* ATG, and inserting it into pN_Nat (30) cut in the same way.

659 *Band shift and gel retardation assays*

660 Probes were PCR-synthesized using oligonucleotides 53 and 92 for the *petE*
661 promoter (217 bp), 299 and 262 for the *petJ* promoter (103 bp), and 295 and 296

662 for *slr0601* (177 bp), introducing a *Sal*I restriction site in all cases. The resulting
663 DNA was digested with *Sal*I and end-labeled with [α-32P]-dCTP (3000 Ci mmol^{-1}
664) using Sequenase v2.0 (Product #70775Y, Affymetrix). The binding reaction
665 was carried out in a final volume of 20 µL containing 4 ng of labeled DNA and 4
666 µg of salmon sperm DNA in 20 mM TRIS-HCl (pH 8.0), 150 mM KCl, 10 mM
667 DTT, 1 mM EDTA, 10% glycerol, and different amounts (from 0.001 µg to 1 µg)
668 of purified PetR. The mixtures were incubated for 30 min at room temperature
669 and loaded on a Tris/Borate/EDTA (TBE) buffer non-denaturing 6%
670 polyacrylamide gel (acrylamide:bisacrylamide 30:0.6). Electrophoresis was
671 carried out at 4ºC and 200 V in 0.25× TBE. Gels were transferred to a Whatman
672 3 MM paper, dried, and autoradiographed using a Cyclone Phosphor System
673 (Packard). Each experiment was performed at least three times with two
674 independent PetR preparations.

675 *RNA-seq*

676 The quantity and quality of total RNA were evaluated using RNA
677 electropherograms acquired by an Agilent 2100 Bioanalyzer; Agilent
678 Technologies, Santa Clara, CA, USA), and library construction of cDNA
679 molecules was carried out using Illumina Kapa Stranded Total RNA with a Ribo-
680 Zero Library Preparation Kit. The resulting DNA fragments (DNA library) were
681 sequenced on an Illumina HiSeq 4000 platform using 150-bp paired-end
682 sequencing reads. Sequencing was carried out by STAB VIDA (Lda, Lisbon,
683 Portugal). Reads were aligned against the NCBI genome sequence for

Synechocystis (NC_000911.1, NC_005229.1, NC_005230.1, NC_005231.1, and NC_005232.1) using bowtie2 version 2.2.4 (55). Raw read counts were calculated using the HTSeq-count function of HTSeq framework 0.11.0 (56). The Bioconductor DESeq2 R software package (57) was used to detect differentially expressed genes. An adjusted *p*-value of <0.01 was considered significant. For RNA-seq density profiles, data were normalized using the BamCoverage function of DeepTools2 0.8.0 (58), and visualized with Integrative Genomics Viewer (IGV) 2.3.6 (59). The RNA-seq dataset is available at GEO accession GSE155385.

Phylogenomic analysis

16S RNA from 169 cyanobacterial genomes (Supplementary Material S1; all completed genomes from NCBI and those included in (60)) were aligned with MUSCLE 3.8.31, and a maximum likelihood (ML) phylogeny was estimated with IQ-TREE 1.6.11 (61) using the best-fitting model (automatically selected by the ModelFinder function) and selecting the phylogeny with the highest likelihood from those found among independent searches, with 1000 bootstrap replicates. *petE, petJ, petR*, and *petP* genes were searched using TBLASTN. Only hits with ≥50% query coverage and >25% identity were considered homologues, and checked manually. Phylogenetic trees were displayed and edited using the Interactive Tree Of Life webtool iTOL v4 (62).

Oxygen evolution

Oxygen evolution was measured by a Clark-type oxygen electrode (Hansatech Chlorolab 2) using mid-logarithmic (OD_{750nm} = 0.8–1) cultures adjusted to OD_{750nm} = 0.5 in BG11C or BG11C-Cu+BCSA media supplemented with 20 mM $NaHCO_3$ and white LED light.

Acknowledgments

We thank Jose Luis Crespo, Manuel J. Mallén, Miguel Roldán, and Sandra Díaz-Troya for critical reading of the manuscript. This research was funded by grant numbers BIO2016-75634-P and PID2019-104513GB-I00 from the Ministerio de Economía y Competividad (MINECO) and the Agencia Estatal de Investigación (AEI), respectively, and by Junta de Andalucía Group BIO-284, co-financed by European Regional Funds (FEDER), to Francisco J. Florencio. RMGC is the recipient of a predoctoral contract from Ministerio de Educación, Cultura y Deporte, Spain (contract #FPU2015/05025).

References

1. Schirrmeister BE, de Vos JM, Antonelli A, Bagheri HC (2013) Evolution of multicellularity coincided with increased diversification of cyanobacteria and the Great Oxidation Event. *Proc Natl Acad Sci U S A* 110(5):1791–6.

2. Koehler MC, Buick R, Kipp MA, Stüeken EE, Zaloumis J (2018) Transient surface ocean oxygenation recorded in the ~2.66-Ga Jeerinah Formation, Australia. *Proc Natl Acad Sci U S A* 115(30):7711–7716.

3. Fischer WW, Hemp J, Johnson JE (2016) Evolution of Oxygenic Photosynthesis. *Annu Rev Earth Planet Sci* 44(1):647–683.

4. Alcott LJ, Mills BJW, Poulton SW (2019) Stepwise Earth oxygenation is an inherent property of global biogeochemical cycling. *Science* 366(6471):1333–1337.

5. Hamilton TL (2019) The trouble with oxygen: The ecophysiology of extant phototrophs and implications for the evolution of oxygenic photosynthesis. *Free Radic Biol Med* 140:233–249.

6. Fischer WW, Hemp J, Valentine JS (2016) How did life survive Earth's great oxygenation? *Curr Opin Chem Biol* 31:166–178.

7. Ilbert M, Bonnefoy V (2013) Insight into the evolution of the iron oxidation pathways. *Biochim Biophys Acta - Bioenerg* 1827(2):161–175.

8. Crichton RR (2019) *Biological inorganic chemistry : a new introduction to molecular structure and function* (Academic Press, London).

9. Tortell PD, Maldonado MT, Granger J, Price NM (1999) Marine bacteria and biogeochemical cycling of iron in the oceans. *FEMS Microbiol Ecol* 29(1):1–11.

10. Behrenfeld MJ, Kolber ZS (1999) Widespread iron limitation of phytoplankton in the south pacific ocean. *Science* 283(5403):840–843.

11. Finazzi G, Sommer F, Hippler M (2005) Release of oxidized plastocyanin from photosystem I limits electron transfer between photosystem I and cytochrome b6f in vivo. *Proc Natl Acad Sci U S A* 102(19):7031–7036.

12. Weigel M, et al. (2003) Plastocyanin is indispensable for photosynthetic electron flow in *Arabidopsis thaliana*. *J Biol Chem* 278(33):31286–9.

13. Sandmann G, Böger P (1980) Copper-induced exchange of plastocyanin and cytochrome c-533 in cultures of *Anabaena variabilis* and *Plectonema boryanum*. *Plant Sci Lett* 17(4):417–424.

14. Sandmann G (1986) Formation of plastocyanin and cytochrome c-553 in different species of blue-green algae. *Arch Microbiol* 145(1):76–79.

15. WOOD PM (1978) Interchangeable Copper and Iron Proteins in Algal Photosynthesis: Studies on Plastocyanin and Cytochrome c-552 in Chlamydomonas. *Eur J Biochem* 87(1):9–19.

16. Kropat J, et al. (2005) A regulator of nutritional copper signaling in *Chlamydomonas* is an SBP domain protein that recognizes the GTAC core of copper response element. *Proc Natl Acad Sci U S A* 102(51):18730–18735.

17. Sommer F, et al. (2010) The CRR1 nutritional copper sensor in chlamydomonas contains two distinct metal-responsive domains. *Plant Cell* 22(12):4098–4113.

765 18. Zhang L, McSpadden B, Pakrasi HB, Whitmarsh J (1992) Copper-
766 mediated regulation of cytochrome c553 and plastocyanin in the
767 cyanobacterium *Synechocystis* 6803. *J Biol Chem* 267(27):19054–19059.

768 19. Ghassemian M, Wong B, Ferreira F, Markley JL, Straus NA (1994)
769 Cloning, sequencing and transcriptional studies of the genes for
770 cytochrome c-553 and plastocyanin from Anabaena sp. PCC 7120.
771 *Microbiology* 140(5):1151–9.

772 20. Van der Plas J, et al. (1989) The gene for the precursor of plastocyanin
773 from the cyanobacterium *Anabaena* sp. PCC 7937: isolation, sequence
774 and regulation. *Mol Microbiol* 3(3):275–84.

775 21. Briggs LM, Pecoraro VL, McIntosh L (1990) Copper-induced expression,
776 cloning, and regulatory studies of the plastocyanin gene from the
777 cyanobacterium *Synechocystis* sp. PCC 6803. *Plant Mol Biol* 15(4):633–
778 42.

779 22. Buikema WJ, Haselkorn R (2001) Expression of the *Anabaena* hetR gene
780 from a copper-regulated promoter leads to heterocyst differentiation under
781 repressing conditions. *Proc Natl Acad Sci U S A* 98(5):2729–2734.

782 23. Tous C, Vega-Palas MA, Vioque A (2001) Conditional expression of
783 RNase P in the cyanobacterium *Synechocystis* sp. PCC6803 allows
784 detection of precursor RNAs. Insight in the in vivo maturation pathway of
785 transfer and other stable RNAs. *J Biol Chem* 276(31):29059–29066.

24. Georg J, et al. (2017) Acclimation of Oxygenic Photosynthesis to Iron Starvation Is Controlled by the sRNA IsaR1. *Curr Biol* 27(10):1425-1436.e7.

25. Giner-Lamia J, et al. (2012) The CopRS Two-Component System Is Responsible for Resistance to Copper in the Cyanobacterium *Synechocystis* sp. PCC 6803. *Plant Physiol* 159(4):1806–1818.

26. Giner-Lamia J, López-Maury L, Florencio FJFJ (2016) Ni interferes in the Cu-regulated transcriptional switch petJ/petE in *Synechocystis* sp. PCC 6803. *FEBS Lett* 590(20):3639–3648.

27. Giner-Lamia J, López-Maury L, Florencio FJ (2014) Global transcriptional profiles of the copper responses in the cyanobacterium *Synechocystis* sp. PCC 6803. *PLoS One* 9(9):e108912.

28. Foster AW, Patterson CJ, Pernil R, Hess CR, Robinson NJ (2012) Cytosolic Ni(II) sensor in cyanobacterium: Nickel detection follows nickel affinity across four families of metal sensors. *J Biol Chem* 287(15):12142–12151.

29. Liu T, et al. (2004) A novel cyanobacterial SmtB/ArsR family repressor regulates the expression of a CPx-ATPase and a metallothionein in response to both Cu(I)/Ag(I) and Zn(II)/Cd(II). *J Biol Chem* 279(17):17810–8.

30. Giner-Lamia J, López-Maury L, Florencio FJ (2015) CopM is a novel copper-binding protein involved in copper resistance in *Synechocystis* sp. PCC 6803. *Microbiologyopen* 4(1):167–185.

31. Krogh A, Larsson B, Von Heijne G, Sonnhammer ELL (2001) Predicting transmembrane protein topology with a hidden Markov model: Application to complete genomes. *J Mol Biol* 305(3):567–580.

32. Peacock SJ, Paterson GK (2015) Mechanisms of Methicillin Resistance in *Staphylococcus aureus*. *Annu Rev Biochem* 84(1):577–601.

33. Durán R V, Hervás M, De La Rosa MA, Navarro JA (2004) The efficient functioning of photosynthesis and respiration in *Synechocystis* sp. PCC 6803 strictly requires the presence of either cytochrome c6 or plastocyanin. *J Biol Chem* 279(8):7229–33.

34. Zhang L, Pakrasi HB, Whitmarsh J (1994) Photoautotrophic growth of the cyanobacterium *Synechocystis* sp. PCC 6803 in the absence of cytochrome c553 and plastocyanin. *J Biol Chem* 269(7):5036–5042.

35. Lambrecht SJ, Steglich C, Hess WR (2020) A minimum set of regulators to thrive in the ocean. *FEMS Microbiol Rev* 44(2):232–252.

36. Pence MA, et al. (2015) Beta-lactamase repressor BlaI modulates *Staphylococcus aureus* cathelicidin antimicrobial peptide resistance and virulence. *PLoS One* 10(8). doi:10.1371/journal.pone.0136605.

826 37. Sala C, et al. (2009) Genome-wide regulon and crystal structure of BlaI
827 (Rv1846c) from *Mycobacterium tuberculosis*. *Mol Microbiol* 71(5):1102–16.

828 38. Seo SW, et al. (2014) Deciphering Fur transcriptional regulatory network
829 highlights its complex role beyond iron metabolism in *Escherichia coli*. *Nat*
830 *Commun* 5:4910.

831 39. Pinochet-Barros A, Helmann JD (2020) Bacillus subtilis Fur is a
832 transcriptional activator for the PerR-repressed *pfeT* gene encoding an iron
833 efflux pump. *J Bacteriol* 202(8):e00697-19.

834 40. Delany I, Rappuoli R, Scarlato V (2004) Fur functions as an activator and
835 as a repressor of putative virulence genes in *Neisseria meningitidis*. *Mol*
836 *Microbiol* 52(4):1081–1090.

837 41. Glauninger H, et al. (2017) Metal-dependent allosteric activation and
838 inhibition on the same molecular scaffold: The copper sensor CopY from:
839 *Streptococcus pneumoniae*. *Chem Sci* 9(1):105–118.

840 42. Belluzo BS, et al. (2019) An experiment-informed signal transduction
841 model for the role of the *Staphylococcus aureus* MecR1 protein in β-lactam
842 resistance. *Sci Rep* 9(1):19558.

843 43. Llarrull LI, Toth M, Champion MM, Mobashery S (2011) Activation of BlaR1
844 protein of methicillin-resistant *Staphylococcus aureus*, its proteolytic
845 processing, and recovery from induction of resistance. *J Biol Chem*

286(44):38148–38158.

44. Staude MW, et al. (2015) Investigation of signal transduction routes within the sensor/transducer protein BlaR1 of *Staphylococcus aureus*. *Biochemistry* 54(8):1600–10.

45. Tottey S, et al. (2012) Cyanobacterial metallochaperone inhibits deleterious side reactions of copper. *Proc Natl Acad Sci U S A* 109(1):95–100.

46. Tottey S, et al. (2008) Protein-folding location can regulate manganese-binding versus copper- or zinc-binding. *Nature* 455(7216):1138–42.

47. Tottey S, Rich PR, Rondet SA, Robinson NJ (2001) Two Menkes-type atpases supply copper for photosynthesis in Synechocystis PCC 6803. *J Biol Chem* 276(23):19999–20004.

48. Castruita M, et al. (2011) Systems biology approach in Chlamydomonas reveals connections between copper nutrition and multiple metabolic steps. *Plant Cell* 23(4):1273–1292.

49. Wang X-Q, Jiang H-B, Zhang R, Qiu B-S (2013) Inactivation of the *petE* gene encoding plastocyanin causes different photosynthetic responses in cyanobacterium *Synechocystis* PCC 6803 under light-dark photoperiod and continuous light conditions. *FEMS Microbiol Lett* 341(2):106–114.

50. Ardelean I, Matthijs HC., Havaux M, Joset F, Jeanjean R (2002)

Unexpected changes in photosystem I function in a cytochrome c 6 - deficient mutant of the cyanobacterium *Synechocystis* PCC 6803. *FEMS Microbiol Lett* 213(1):113–119.

51. Ivanov AG, et al. (2012) Restricted capacity for PSI-dependent cyclic electron flow in ΔpetE mutant compromises the ability for acclimation to iron stress in *Synechococcus* sp. PCC 7942 cells. *Biochimica et Biophysica Acta - Bioenergetics*, pp 1277–1284.

52. Stanier RY, Deruelles J, Rippka R, Herdman M, Waterbury JB (1979) Generic Assignments, Strain Histories and Properties of Pure Cultures of Cyanobacteria. *Microbiology* 111(1):1–61.

53. García-Domínguez M, Florencio FJ (1997) Nitrogen availability and electron transport control the expression of *glnB* gene (encoding PII protein) in the cyanobacterium *Synechocystis* sp. PCC 6803. *Plant Mol Biol* 35(6):723–734.

54. J.F. S, Russell D (2001) *Molecular Cloning: A Laboratory Manual (3-Volume Set)*.

55. Langmead B, Salzberg SL (2012) Fast gapped-read alignment with Bowtie 2. *Nat Methods* 9(4):357–359.

56. Anders S, Pyl PT, Huber W (2015) Genome analysis HTSeq-a Python framework to work with high-throughput sequencing data. 31(2):166–169.

886 57. Love MI, Huber W, Anders S (2014) Moderated estimation of fold change
887 and dispersion for RNA-seq data with DESeq2. *Genome Biol* 15(12).
888 doi:10.1186/s13059-014-0550-8.

889 58. Ramírez F, et al. (2016) deepTools2: a next generation web server for
890 deep-sequencing data analysis. *Nucleic Acids Res* 44(W1):W160–W165.

891 59. Robinson JT, et al. (2011) Integrative genomics viewer. *Nat Biotechnol*
892 29(1):24–26.

893 60. Shih PM, et al. (2013) Improving the coverage of the cyanobacterial
894 phylum using diversity-driven genome sequencing. *Proc Natl Acad Sci U S*
895 *A* 110(3):1053–1058.

896 61. Nguyen L-T, Schmidt HA, Von Haeseler A, Minh BQ (2015) IQ-TREE: A
897 Fast and Effective Stochastic Algorithm for Estimating Maximum-Likelihood
898 Phylogenies. *Mol Biol Evol* 32(1):268–274.

899 62. Letunic I, Bork P (2019) Interactive Tree Of Life (iTOL) v4: recent updates
900 and new developments. *Web Serv issue Publ online* 47(W1):W256–W259.

901

902

Figure Legends

Figure 1. PetRP regulatory system controls *petJ*/*petE* switch in *Synechocystis* sp. PCC 6803.

A. RNA blot analysis of *petJ, petE* and *copM* in WT, PETR and PETP strains in response to 0.5 μM copper addition. Total RNA was isolated from cells grown in BG11C-Cu medium at the indicated times after addition of 0.5 μM of copper. The filters were hybridized with *petJ*, *petE* and *copM* probes and subsequently stripped and re-hybridized with a *rnpB* probe as a control.

B. Immunoblot analysis of Cytc_6, PC, CopM and GSI in WT, PETR and PETP strains in response to 0.5 μM copper addition. Cells were grown in BG11C-Cu medium and cells were harvested at the indicated times addition of 0.5 μM of copper. 5 μg of total protein from soluble extracts was separated by 15 % SDS-PAGE and subjected to inmunoblot to detect PC, Cytc_6,CopM or GSI.

C. Quantification of PC levels in WT, PETR and PETP strains grown in BG11C-Cu +BCSA (blue bars), BG11C-Cu (orange bars) or BG11C (grey bars). 10 μg of total soluble proteins were loaded and compared to serial dilutions (100%, 50%, 25% and 12.5%) of the WT extract prepared from cells grown in BG11C. Data are the mean ± SE of three biologically independent experiments. Asterisk indicate significant difference to WT in the same condition (*t*-test; $p<0.05$).

925 D. Quantification of Cytc_6 levels in WT, PETR and PETP strains grown in
926 BG11C-Cu +BCSA (blue bars), BG11C-Cu (orange bars) or BG11C (grey
927 bars). 10 µg of total soluble proteins were loaded and compared to serial
928 dilutions (100%, 50%, 25% and 12.5%) of the WT extract prepared from
929 cells grown in BG11C-Cu+BCSA. Data are the mean ± SE of three
930 biologically independent experiments. Asterisk indicate significant
931 difference to WT in the same condition (*t*-test; $p<0.05$).
932
933 **Figure 2. PetP is a copper activated protease that regulates PetR levels.**
934 A. Immunoblot analysis of PetR in WT, PETR and PETP strains in response
935 to 0.5 µM copper addition. Cells were grown in BG11C-Cu medium and
936 harvested at the indicated times after addition of 0.5 µM of copper. Whole
937 cells were loaded (0.2 OD_{750nm}), separated by 15 % SDS-PAGE and
938 subjected to immunoblot to detect PetR or GSI as loading control.
939 B. Immunoblot analysis of Cytc_6, PC and PetR in WT, PETR and PETP
940 strains grown in BG11C-Cu+BCSA (B), BG11C-Cu (-) or BG11C. 10 µg of
941 total soluble proteins were separated by 15 % SDS-PAGE and subjected
942 to immunoblot blot to detect PC, Cytc_6, or GSI as loading control. For PetR
943 whole cell extracts were used and 20 µl (equivalent to 0.2 OD_{750nm}) were
944 loaded per lane.
945 C. Quantification of PetR levels in WT, PETR and PETP strains grown in
946 BG11C-Cu +BCSA (blue bars), BG11C-Cu (orange bars) or BG11C (grey
947 bars). 20 µl of the whole cells extract were loaded and compared to serial

dilutions (100%, 50%, 25% and 12.5%) of the WT extract prepared from cells grown in BG11C-Cu+BCSA. Data are the mean ± SE of three biologically independent experiments. Asterisk indicate significant difference to WT in the same condition (*t*-test; $p>0.05$).

D. GST-PetR was incubated for the indicated time with total extracts prepared from WT, PETR and PETP strains grown in BG11C-Cu. 0.5 µM $CuSO_4$ was added to the extracts as indicated. Samples were taken at the indicated times, mixed with Laemmli buffer, boiled, separated in 12% SDS-PAGE gels and GST-PetR was detected using PetR antibodies.

E. GST-PetR was incubated for the indicated time with whole cell extracts prepared from *E. coli* carrying pN_petRP or pN_Nat (an empty plasmid) grown in M9 minimal media. 0.5 µM $CuSO_4$ was added to the extracts as indicated. Samples were taken at the indicated times, mixed with Laemmli buffer, boiled, separated in 12% SDS-PAGE gels and GST-PetR was detected using PetR antibodies

Figure 3. PetR binds to *petJ* and *petE* promoters.

A. Electrophoretic mobility shift assay using recombinant PetR to a 103 bp *petJ* promoter probe. The indicated PetR concentration were used in each lane.

B. Electrophoretic mobility shift assay using recombinant PetR to a 217 bp *petE* promoter probe. The indicated PetR concentration were used in each lane.

C. Sequence logo identified with MEME using upstream sequences (300 bp) from *petE* and *petJ* genes from genomes that also contained *petRP*.

D. Sequence logo identified with MEME using upstream sequences (300 bp) from *petJ* genes from genomes that also contained *petRP*.

E. Sequence logo identified with MEME using upstream sequences (300 bp) from *petE* from genomes that also contained *petRP*.

F. Alignment of the *petJ* and *petE* promoter sequences from *Synechocystis*. Transcriptional start sites are in capital letters and underlined, -10 boxes are yellow underlined and conserved nucleotides from the motif found in C are in red.

Figure 4. Physiological characterization of *petR* and *petP* mutant strains.

A. Growth of WT, PETE, PETJ, PETR, PETP and PETRP strains in different copper availability regimes. Tenfold serial dilutions of a 1 µg chlorophyll mL^{-1} cells suspension were spotted onto BG11C-Cu+BCSA, BG11C-Cu o BG11C. Plates were photographed after 5 days of growth

B. Oxygen evolution measured using a Clark electrode at increasing light intensities in exponential growing cultures (OD_{750nm}= 0.5-1) of WT (●), PETJ (●), PETE (●), PETR (●) and PETP (●) strains grown in BG11C-Cu+BCSA. Data are the mean ± SE of at least three biologically independent experiments.

C. Oxygen evolution measured using a Clark electrode at increasing light intensities in exponential growing cultures (OD_{750nm}= 0.5-1) of WT (●),

PETJ (●), PETE (●), PETR (●) and PETP (●) strains grown in BG11C. Data are the mean ± SE of at least three biologically independent experiments.

Figure 5. Model of the regulatory mechanism for *petE*/*petJ* switch mediated by PetRP.

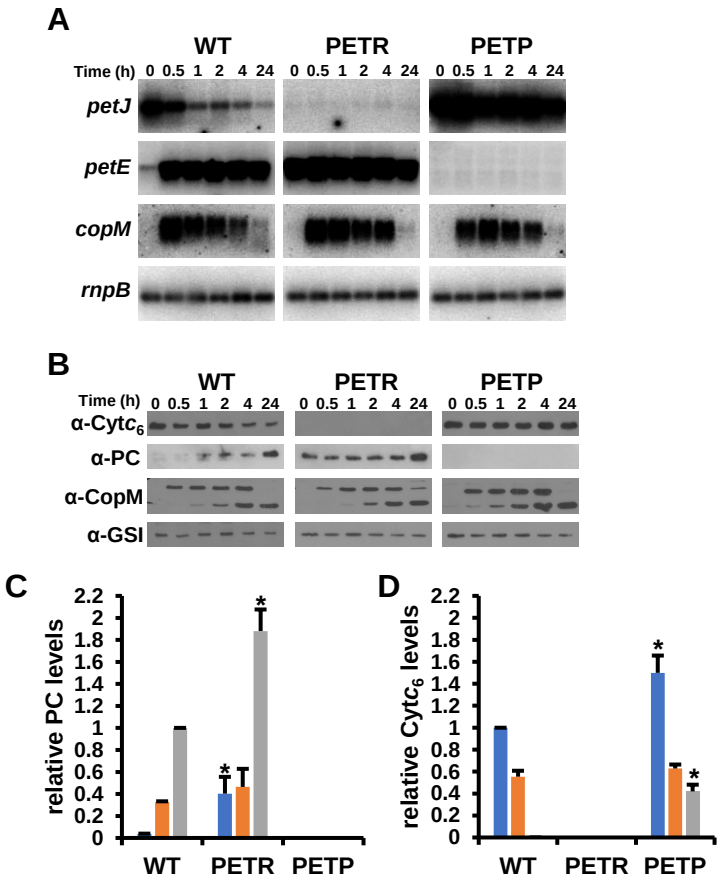

Figure 1. PetRP regulatory system controls *petJ*/*petE* switch in *Synechocystis* sp. PCC 6803.

A. RNA blot analysis of *petJ, petE* and *copM* in WT, PETR and PETP strains in response to 0.5 µM copper addition. Total RNA was isolated from cells grown in BG11C-Cu medium at the indicated times after addition of 0.5 µM of copper. The filters were hybridized with *petJ*, *petE* and *copM* probes and subsequently stripped and re-hybridized with a *rnpB* probe as a control.

B. Immunoblot analysis of Cytc_6, PC, CopM and GSI in WT, PETR and PETP strains in response to 0.5 µM copper addition. Cells were grown in BG11C-Cu medium and cells were harvested at the indicated times addition of 0.5 µM of copper. 5 µg of total protein from soluble extracts was separated by 15 % SDS-PAGE and subjected to inmunoblot to detect PC, Cytc_6,CopM or GSI.

C. Quantification of PC levels in WT, PETR and PETP strains grown in BG11C-Cu +BCSA (blue bars), BG11C-Cu (orange bars) or BG11C (grey bars). 10 µg of total soluble proteins were loaded and compared to serial dilutions (100%, 50%, 25% and 12.5%) of the WT extract prepared from cells grown in BG11C. Data are the mean ± SE of three biologically independent experiments. Asterisk indicate significant difference to WT in the same condition (*t*-test; $p<0.05$).

D. Quantification of Cytc_6 levels in WT, PETR and PETP strains grown in BG11C-Cu +BCSA (blue bars), BG11C-Cu (orange bars) or BG11C (grey bars). 10 µg of total soluble proteins were loaded and compared to serial dilutions (100%, 50%, 25% and 12.5%) of the WT extract prepared from cells grown in BG11C-Cu+BCSA. Data are the mean ± SE of three biologically independent experiments. Asterisk indicate significant difference to WT in the same condition (*t*-test; $p<0.05$).

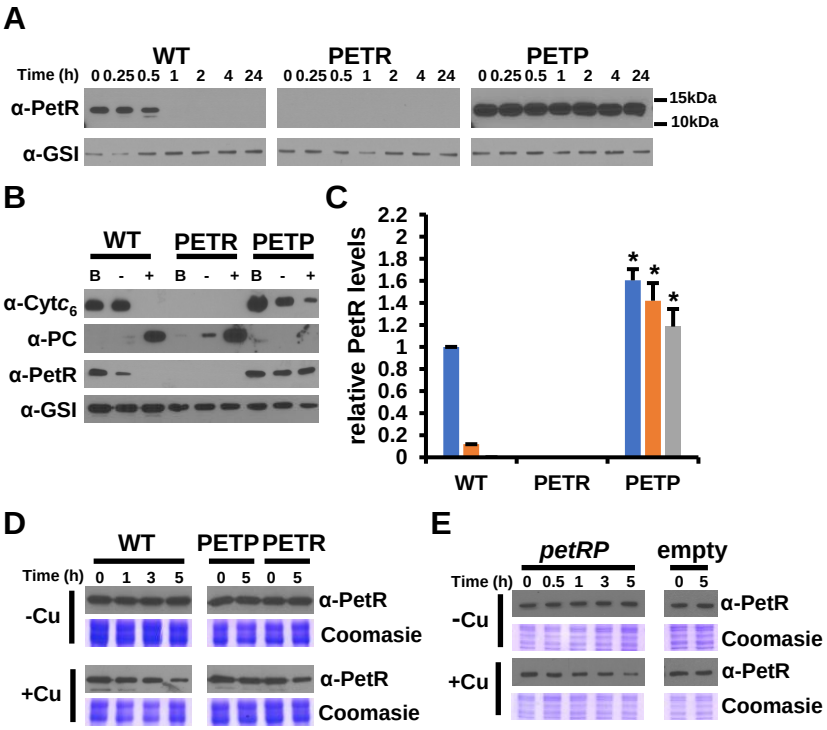

Figure 2. PetP is a copper activated protease that regulates PetR levels.

A. Immunoblot analysis of PetR in WT, PETR and PETP strains in response to 0.5 µM copper addition. Cells were grown in BG11C-Cu medium and harvested at the indicated times after addition of 0.5 µM of copper. Whole cells were loaded (0.2 OD_{750nm}), separated by 15 % SDS-PAGE and subjected to immunoblot to detect PetR or GSI as loading control.

B. Immunoblot analysis of Cytc_6, PC and PetR in WT, PETR and PETP strains grown in BG11C-Cu+BCSA (B), BG11C-Cu (-) or BG11C. 10 µg of total soluble proteins were separated by 15 % SDS-PAGE and subjected to immunoblot blot to detect PC, Cytc_6, or GSI as loading control. For PetR whole cell extracts were used and 20 µl (equivalent to 0.2 OD_{750nm}) were loaded per lane.

C. Quantification of PetR levels in WT, PETR and PETP strains grown in BG11C-Cu +BCSA (blue bars), BG11C-Cu (orange bars) or BG11C (grey bars). 20 µl of the whole cells extract were loaded and compared to serial dilutions (100%, 50%, 25% and 12.5%) of the WT extract prepared from cells grown in BG11C-Cu+BCSA. Data are the mean ± SE of three biologically independent experiments. Asterisk indicate significant difference to WT in the same condition (*t*-test; $p>0.05$).

D. GST-PetR was incubated for the indicated time with total extracts prepared from WT, PETR and PETP strains grown in BG11C-Cu. 0.5 µM $CuSO_4$ was added to the extracts as indicated. Samples were taken at the indicated times, mixed with Laemmli buffer, boiled, separated in 12% SDS-PAGE gels and GST-PetR was detected using PetR antibodies.

E. GST-PetR was incubated for the indicated time with whole cell extracts prepared from *E. coli* carrying pN_petRP or pN_Nat (an empty plasmid) grown in M9 minimal media. 0.5 µM $CuSO_4$ was added to the extracts as indicated. Samples were taken at the indicated times, mixed with Laemmli buffer, boiled, separated in 12% SDS-PAGE gels and GST-PetR was detected using PetR antibodies.

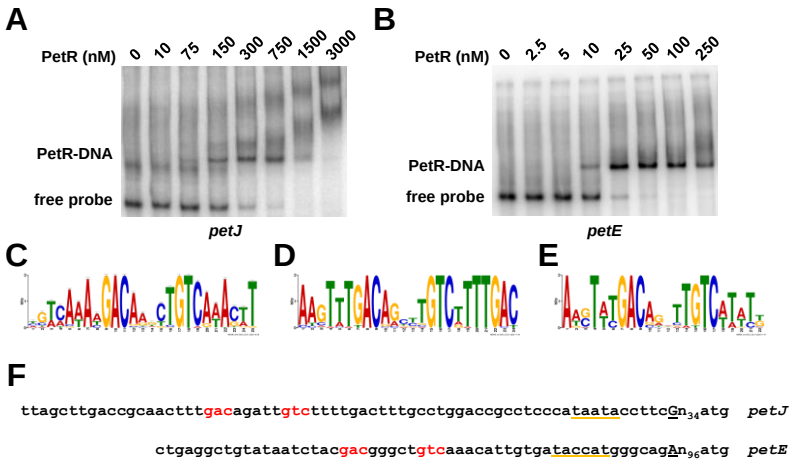

Figure 3. PetR binds to *petJ* and *petE* promoters.

A. Electrophoretic mobility shift assay using recombinant PetR to a 103 bp *petJ* promoter probe. The indicated PetR concentration were used in each lane.
B. Electrophoretic mobility shift assay using recombinant PetR to a 217 bp *petE* promoter probe. The indicated PetR concentration were used in each lane.
C. Sequence logo identified with MEME using upstream sequences (300 bp) from *petE* and *petJ* genes from genomes that also contained *petRP*.
D. Sequence logo identified with MEME using upstream sequences (300 bp) from *petJ* genes from genomes that also contained *petRP*.
E. Sequence logo identified with MEME using upstream sequences (300 bp) from *petE* from genomes that also contained *petRP*.
F. Alignment of the *petJ* and *petE* promoter sequences from *Synechocystis*. Transcriptional start sites are in capital letters and underlined, -10 boxes are yellow underlined and conserved nucleotides from the motif found in C are in red.

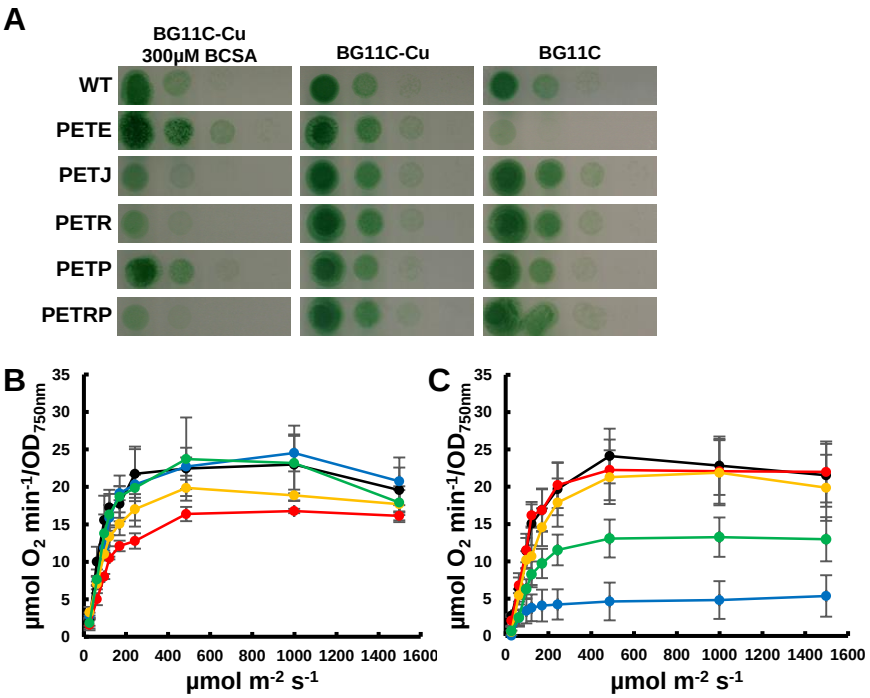

Figure 4. Physiological characterization of *petR* and *petP* mutant strains.

A. Growth of WT, PETE, PETJ, PETR, PETP and PETRP strains in different copper availability regimes. Tenfold serial dilutions of a 1 µg chlorophyll mL^{-1} cells suspension were spotted onto BG11C-Cu+BCSA, BG11C-Cu o BG11C. Plates were photographed after 5 days of growth

B. Oxygen evolution measured using a Clark electrode at increasing light intensities in exponential growing cultures (OD_{750nm}= 0.5-1) of WT (●), PETJ (●), PETE (●), PETR (●) and PETP (●) strains grown in BG11C-Cu+BCSA. Data are the mean ± SE of at least three biologically independent experiments.

C. Oxygen evolution measured using a Clark electrode at increasing light intensities in exponential growing cultures (OD_{750nm}= 0.5-1) of WT (●), PETJ (●), PETE (●), PETR (●) and PETP (●) strains grown in BG11C. Data are the mean ± SE of at least three biologically independent experiments.

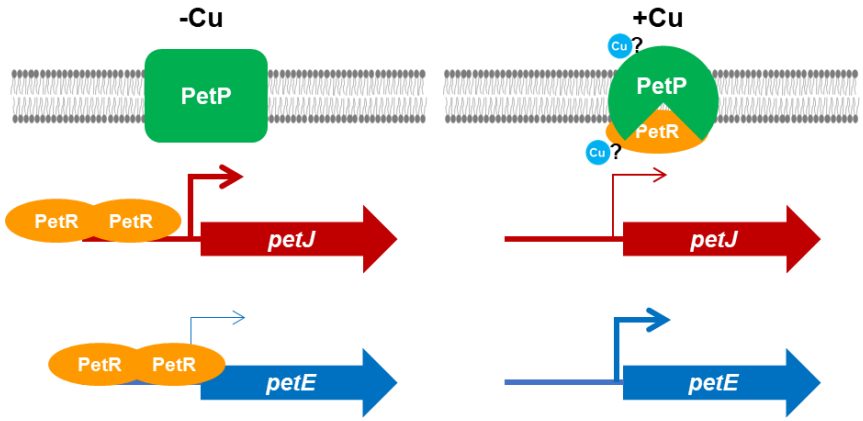

Figure 5. Model of the regulatory mechanism for *petE*/*petJ* switch mediated by PetRP.